

# Aggregation-Induced Fast Crystal Growth of SnO<sub>2</sub> Nanocrystals

Zanyong Zhuang,<sup>†</sup> Feng Huang,<sup>‡</sup> Zhang Lin,<sup>\*,†</sup> and Hengzhong Zhang<sup>\*,§</sup>

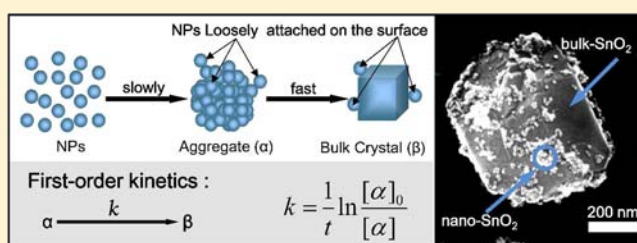
<sup>†</sup>State Key Laboratory of Structures, Fujian Institute of Research on the Structure of Matter, Chinese Academy of Sciences, Fuzhou, Fujian, 350002, China

<sup>‡</sup>Key Laboratory of Optoelectronic Materials Chemistry and Physical Chemistry, Fujian Institute of Research on the Structure of Matter, Chinese Academy of Sciences, Fuzhou, Fujian, 350002, China

<sup>§</sup>Department of Earth and Planetary Science, University of California, Berkeley, California 94720, United States

## Supporting Information

**ABSTRACT:** In this paper, we report an ultrafast growth of SnO<sub>2</sub> nanocrystals directly from ~4 to ~350 nm in a hydrothermal process (250 °C, time >180 h). The crystal growth system is characterized by “either small or large” particle size; that is, only two differently sized SnO<sub>2</sub> particles, either several nanometers or ~350 nm, coexist. During the fast growth process, SnO<sub>2</sub> nanoparticles assembled to form densely aggregated aggregates that can quickly transform to big (bulk-like) crystals. The kinetic analysis, for the first time, point out that the fast growth reaction (from nanocrystal aggregates to bulk-like crystals) follows a first-order reaction law with a very large kinetic pre-exponent factor ( $1.53 \times 10^{27} \text{ h}^{-1}$ ), which is in line with our proposed aggregation-induced fast crystal growth mechanism. Small-angle X-ray scattering (SAXS) study of the aggregates supports that the onset of the fast growth is closely related to an increase in the aggregation degree of the aggregates. Moreover, disintegrating the aggregation state via introduction of other particles (Al<sub>2</sub>O<sub>3</sub>) into the system prohibited the fast growth. The finding in this work provides new threads for syntheses of novel nanomaterials that may possess properties not readily obtained via conventional crystal growth routes.



## INTRODUCTION

An in-depth understanding of crystal growth mechanisms and kinetics provides guidance for particle size control during nanomaterial synthesis.<sup>1–4</sup> Principally, the descriptions of crystal growths are based on the classical Ostwald Ripening (OR) mechanism<sup>5,6</sup> and the newly discovered Oriented Attachment (OA) mechanism.<sup>7,8</sup> The OR kinetics are characterized by an exponentially growing average particle size,<sup>9</sup> while the OA growth rate can typically be fitted by an asymptotic curve.<sup>7,9,10</sup> Coexistence of the two mechanisms commonly present in material syntheses enables crystals growing continuously in kinetics.<sup>7,9,11</sup> Particle size tailoring ranging from nano- to micrometers can thus be achieved through a continuous kinetic control of growths by, e.g., coarsening temperature and time.<sup>7,9</sup>

Recently, a growing body of experimental work showed that in contrast to the continuous size evolution in OR/OA growths a fast growth directly from nano- to microcrystals was sometimes observed.<sup>12–15</sup> For instance, we previously revealed a fast growth and phase transformation process from the aggregates of 20 nm Mg(OH)<sub>2</sub> to 2 μm Na<sub>2</sub>Mg(CO<sub>3</sub>)<sub>2</sub> crystals.<sup>14</sup> Zhan et al. reported the direct formation of large-crystal CaCO<sub>3</sub> (1 μm) via nanocrystal (20 nm) aggregation.<sup>12</sup> Oriented assembly of small Fe<sub>3</sub>O<sub>4</sub> nanoparticles into hollow single-crystal microspheres<sup>13</sup> and the growth of large-sized Prussian Blue crystals via assembly of nanocrystals were also observed.<sup>15</sup> Representatively, the growth stages are charac-

terized by either small or large crystal sizes,<sup>12–15</sup> wherein the midsize particles are absent. This special growth characteristic has shown to play an important role in the synthesis of advanced functional materials and in natural mineral formations.<sup>16–18</sup> In the past decade, great efforts have been made to probe the underlying mechanism. Usually, it is thought to be associated with an aggregation-based crystal growth mechanism.<sup>16</sup> It is sometimes described by the term “mesocrystal” coined by Cölfen and Mann.<sup>18</sup> In both cases, the growths prove closely related to the aggregates of primary nanounits, the fusion of which forms the single bulk crystal.<sup>14,16–18</sup> Unfortunately, phase transformation frequently accompanies the crystal growth.<sup>14,16,17</sup> This complicity leads to the difficulty in studying the growth mechanism and hence a lack of good understanding of this special growth process. To date, the majority of research is restricted to the investigation of the growth process itself rather than to get comprehensive insights into the kinetics and the underlying mechanism in particular.<sup>14,18</sup> Generally, an understanding of the factors that affect the kinetics is fundamental to tune the crystal growth and thus to achieve new types of nanostructures and new material properties.<sup>7,9</sup>

Tailoring the size of tin oxide (SnO<sub>2</sub>) crystal is of great interest for its wide applications in nanotechnology.<sup>19,20</sup>

Received: June 1, 2012

Published: September 6, 2012

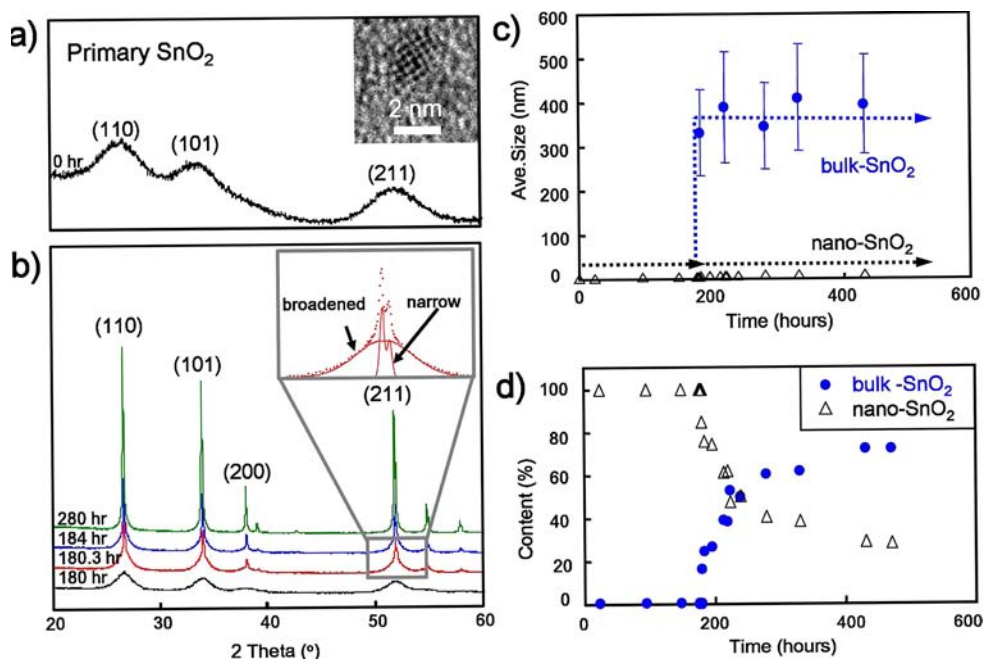


**Figure 1.** (a) XRD pattern and HRTEM image of as-prepared SnO<sub>2</sub> nanoparticles. (b) Time series XRD analysis of SnO<sub>2</sub> treated hydrothermally in water at 250 °C. Abrupt change occurs at a threshold time of 180 h. Inset panel is Gauss fitting of the (211) diffraction peak for SnO<sub>2</sub> treated for 180.3 h by using a pair of broadened and narrow peaks, indicating the coexistence of two differently sized SnO<sub>2</sub>. (c) Rietveld analysis showing the particle size of SnO<sub>2</sub> in sample versus time when treated at 250 °C, demonstrating that following the slow growth is the steep rise of particle size in the second stage. The average size of BCs for all the growth times is  $\sim$ 380 nm. (d) Rietveld analysis showing the relative weight fractions of differently sized SnO<sub>2</sub> versus time.

However, previous kinetic studies indicate that typically SnO<sub>2</sub> particles grow very slowly, limiting the crystal size to only a few nanometers.<sup>10,21,22</sup> For instance, we demonstrated that nano-SnO<sub>2</sub> treated hydrothermally could stabilize at a small particle size for a long time (4.2 nm, 250 °C, 180 h).<sup>10</sup> The slow growth of SnO<sub>2</sub> was attributed to 1 + 1 OA growth kinetics of the primary small particles.<sup>10</sup> In this work, a subsequent steep growth of nanocrystals directly from  $\sim$ 4 to 350 nm was observed after 180 h. Only two differently sized SnO<sub>2</sub> particles coexisted in the system; i.e., they were either several nanometers or  $\sim$ 350 nm. Particles of the sizes in between were hardly found. Fortunately, no phase transformation occurred in this process. Therefore, for the first time, the kinetic rule of particle sizes, structures, and relative weight fractions of both the small and big SnO<sub>2</sub> crystals during the fast growth can be characterized. Systemic kinetic determinations and analyses of the fast size conversion provide insight into an aggregation-induced synergetic fast crystal growth mechanism.

## EXPERIMENTAL SECTION

**Chemicals.** Stannic chloride (SnCl<sub>4</sub>·5H<sub>2</sub>O), aluminum oxide (Al<sub>2</sub>O<sub>3</sub>), and ammonium hydroxide (NH<sub>3</sub>·H<sub>2</sub>O, 28%) are of analytical grade. All chemicals were purchased from Alfa Aesar and used without further purification.

**Preparation of Primary SnO<sub>2</sub> Nanoparticles.** Using a typical procedure after minor modifications,<sup>21,22</sup> SnO<sub>2</sub> nanoparticles were prepared by the hydrolysis of stannic chloride. To an aqueous solution of SnCl<sub>4</sub>·5H<sub>2</sub>O was added NH<sub>3</sub>·H<sub>2</sub>O. At room temperature, a white turbid suspension was produced immediately. No surfactant was used to minimize external effects on the crystal growth in the following. When pH value came to  $\sim$ 5, the suspension was centrifuged at the speed of 8000 rpm for 2 min. The white precipitate was washed repeatedly with distilled water until Cl<sup>-</sup> was beyond the detection by 0.1 M AgNO<sub>3</sub> solution. Finally, the product was dried under 80 °C for

48 h (Sn(OH)<sub>4</sub> → SnO<sub>2</sub> + 2H<sub>2</sub>O) and ground into powder for kinetic measurements.

**Growth Kinetics of SnO<sub>2</sub> Nanoparticles in the Aggregated State.** An amount of primary SnO<sub>2</sub> (0.1 g) and distilled water (10 mL) were loaded into a Teflon-lined stainless steel autoclave with 23 mL capacity. Later, the autoclaves were put in a large oven. Accurate and precise control of the oven temperature at required 250 or 263 °C ensures each autoclave in the oven is thermally equilibrated and hence of the same reaction temperature. For the time series experiment, autoclave containers were taken out at the appropriate time interval and quenched to room temperature with ice water immediately. We placed 2–3 samples for each time point for reducing systematic experimental data errors. To examine the aggregating state of SnO<sub>2</sub> nanoparticles during the coarsening process, a small portion of the suspension was quickly extracted from near the bottom of an autoclave container. The precipitates were centrifuged, dried, and characterized by X-ray diffraction, (XRD), transmission electron microscopy (TEM), and scanning electron microscopy (SEM).

**Growth Kinetics of SnO<sub>2</sub> at a Relatively Scattered State.** Primary SnO<sub>2</sub> particles (0.1 g), Al<sub>2</sub>O<sub>3</sub> (0.1 g), and distilled water (10 mL) were mixed under ultrasonic treatment for over 2 h. After dispersing SnO<sub>2</sub>, the mixed sample was loaded into a Teflon-lined stainless steel autoclave with 23 mL capacity and heated at 250 °C. For the time series experiment, hydrothermal treatment of samples was performed via the same route as above.

**Characterization.** *XRD.* The crystal structures and the average sizes of samples were identified by a PANalytical X'Pert PRO diffractometer with Cu K $\alpha$  radiation (40 kV, 40 mA) in the continuous scanning mode. The scanning range of 2 $\theta$  was from 10° to 120° in steps of 0.02° with a collection time of 35 s per step. The average crystallite size of nanocrystals was calculated from peak broadening by using the Scherrer equation. The large crystallite size (e.g.,  $\sim$ 350 nm) was figured out by SEM statistics. Data processing by the Rietveld refining method was further carried out by using the Fullprof software.

*TEM and SEM.* To confirm the sizes and morphologies of SnO<sub>2</sub> nanoparticles, TEM and SEM images were taken on a JEOL JEM2010 at 200 kV and an LEO 1530 at 200 kV, respectively. All samples were

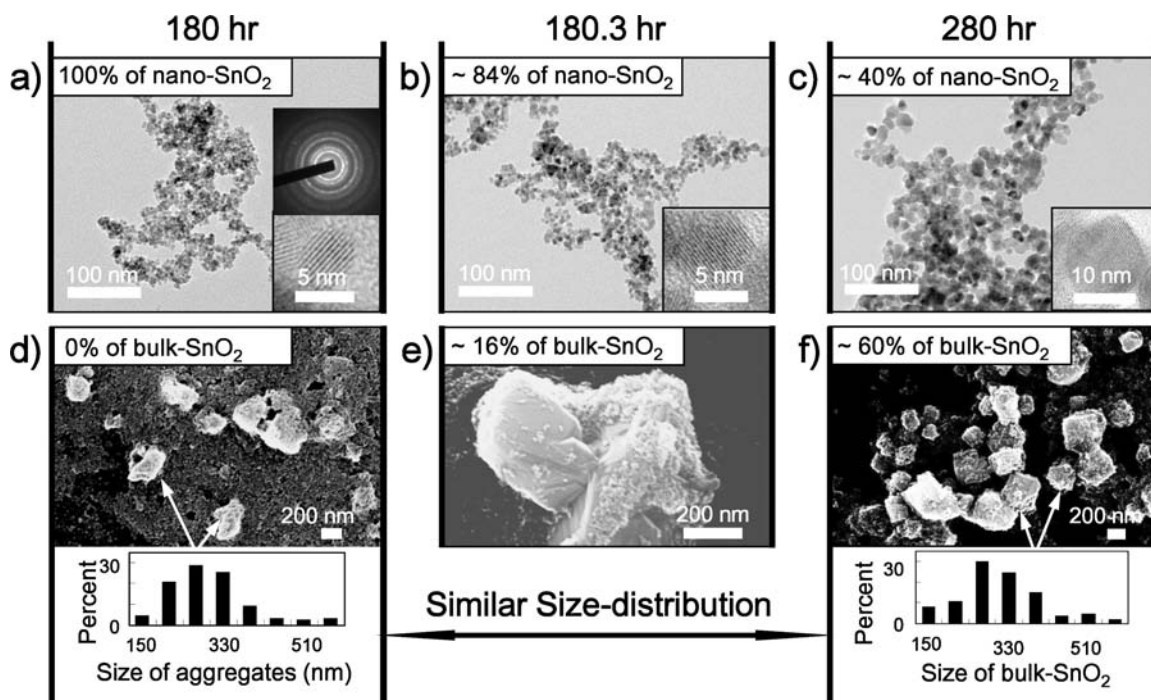


**Figure 2.** Typical TEM (a–c) analysis with high-resolution images showing the small SnO<sub>2</sub> NPs in samples treated hydrothermally in water at 250 °C for 180, 180.3, and 280 h, respectively. Insetted selected area electron diffraction image in panel a implies that the aggregated nanoparticles are randomly oriented. Typical SEM (d–f) images showing large-sized SnO<sub>2</sub>, either aggregates or BCs, in samples treated hydrothermally in water at 250 °C for 180, 180.3, and 280 h, respectively. The underlying histogram in panel d and f showing the statistic size distribution of the original aggregates at 180 h and BCs formed at 280 h collected by SEM. Enlarged images of panel d and f are shown in Figure S3 in the SI. Clearly, the bulk-like SnO<sub>2</sub> crystals have smooth crystal surfaces, distinct face angles, and a higher image resolution when compared to the aggregates.

prepared by depositing a drop of ethanol solution containing the nanocrystals onto holey carbon-coated grids.

**Small-Angle X-ray Scattering (SAXS).** To determine the aggregation state of SnO<sub>2</sub> at different coarsening times, a small portion of the suspension was quickly extracted from near the bottom of an autoclave container as described above. In such a way, the sampled suspension contained structure information of SnO<sub>2</sub> in both the precipitates and the solution. After a dilution, it was characterized by SAXS, using synchrotron radiation as the X-ray source with a long-slit collimation system at the Shanghai Synchrotron Radiation Facility (SSRF). X-rays of 1.24 Å in wavelength were selected and focused to 0.5 × 0.5 mm<sup>2</sup> at the sample with a camera length of 5417 mm. The scattered X-ray intensities were recorded using an image plate. The images were further converted to scattering intensity vs  $q$  (scattering vector) data using the beamline software. Each data collection lasted for ~5–10 min, depending on the strength of the monitored scattering intensity (weak ones used longer times). The absorption of the sample and the background scattering were corrected.

## RESULTS

Figure 1a shows the typical XRD pattern and HRTEM image of as-prepared SnO<sub>2</sub> nanoparticles. The broadened XRD pattern reveals that primary nanoparticles are in the tetragonal phase, with a calculated average size of  $1.9 \pm 0.1$  nm in [110], [101], and [211] directions using the Scherrer equation. HRTEM observation confirmed the size, morphology, and phase structure from the XRD.

SnO<sub>2</sub> nanoparticles coarsened at 250 °C in water were characterized with the same methods as above. During the first 180 h, as revealed in our previous kinetic work,<sup>10</sup> SnO<sub>2</sub> grew slowly from 1.9 to ~4.2 nm, which could be attributed to a typical 1 + 1 OA growth mode. It is worthy to mention that, in this stage, after the first 50 h the growth of SnO<sub>2</sub> has essentially ceased due to its low solubility (see Figure S1 in the Supporting

Information, abbreviated SI). However, as shown in Figure 1b, the growth behavior of SnO<sub>2</sub> over 180 h was totally different. Compared to the broad XRD patterns obtained at/before 180 h, at subsequent 180.3 h a group of extremely narrow peaks related to tetragonal SnO<sub>2</sub> suddenly appeared, indicating the occurrence of a fast crystal growth. Peak separation using the Gauss function (the inset plane in Figure 1b) indicates that two differently sized SnO<sub>2</sub> particles coexisted in this stage. Rietveld refinement (see Figure S2, SI) clearly demonstrates that one part was ~5 nm SnO<sub>2</sub> nanoparticles (NPs), and the other part was large SnO<sub>2</sub> denoted as bulk crystals (BCs) below. For instance, SEM investigation reveals that the average size of BCs at 280 h was up to ~350 nm, with a size distribution ranging from 150 to 510 nm as shown in Figure 2e. Strangely, both extensive SEM and TEM investigation as described in the following part confirm that SnO<sub>2</sub> crystals of intermediate size between ~10 and 100 nm can hardly be found, indicating a steep rise in particle size. Time series experiments (Figure 1b) demonstrate that the XRD pattern of the sample at each sampling time after 180 h was composed of a pair of broadened and narrow peaks. Rietveld analysis, shown in Figure 1c, suggests that all the samples after 180 h share the same characteristic that two differently sized SnO<sub>2</sub> particles coexist (either no more than 10 nm or BCs). Moreover, the relative content of SnO<sub>2</sub> NPs and BCs in the sample changed with time. As shown in Figure 1d, within 0–180 h, 100% of SnO<sub>2</sub> was no more than 5 nm. Merely at 180.3 h, ~16% of NPs fast transformed to BCs, while the residual ~84% remained in the several nanometers region. Between 180 and 280 h, the relative amount of NPs decreased quickly with the obvious increase of BCs. The maximum amount of BCs approached ~75% at

around 430 h. After that, the amount of NPs and BCs in the sample remained at ~25% and ~75%, respectively.

The size and fine structure of SnO<sub>2</sub> NPs and BCs in each sample were further analyzed by TEM and SEM. Three typical images of 180, 180.3, and 280 h are included in Figure 2. Extensive TEM analysis demonstrates that at 180 h all SnO<sub>2</sub> particles were only ~4 nm (Figure 2a), which agrees with the XRD analysis. Systemic SEM investigation (Figure 2d and Figure S3a, SI) clearly demonstrates that a large amount of SnO<sub>2</sub> NPs were highly aggregated to form big aggregates. Size statistics (histogram of Figure 2d) further reflects that these aggregates are of an average size of ~350 nm. Figure S4a and Figure S4b (SI) show, respectively, TEM images and corresponding selected area electron diffraction (SAED) patterns of the nano-SnO<sub>2</sub> aggregate at 180 h. The SAED pattern in Figure S4b (SI) shows typical powder diffraction rings. This confirms the existence of aggregates at 180 h, which consist of a large number of SnO<sub>2</sub> nanoparticles. When reaching 180.3 h, as shown in Figure 2b, TEM analysis shows that mostly SnO<sub>2</sub> particles still stay at ~5.2 nm. This again is in accordance with the above XRD analysis. Similar to the case of 180 h, SEM observations revealed that these SnO<sub>2</sub> NPs existed in the form of aggregates (see Figure S5, SI). However, as shown in Figure 2e, very small amounts of large crystals (about 300–400 nm) were also found, which agrees with the XRD analysis that a small part of BCs emerged. The TEM image at 280 h indicates the existence of SnO<sub>2</sub> NPs with average particle size no more than 10 nm (the size statistics histogram is shown in Figure S6, SI). However, different from the time points of 180 and 180.3 h, only a few aggregates were visible with the SEM (the SEM is more effective to analyze the large crystals than the TEM). Instead, in Figure 2f and Figure S3b (SI), a mass of SnO<sub>2</sub> single crystals with an average size of ~350 nm can be seen. Figure S4c and S4d (SI), respectively, further provide TEM images and SAED patterns of bulk-like SnO<sub>2</sub> crystal at 280 h. The bright spot patterns in Figure S4d (SI) confirm the formation of the bulk-like single-phase SnO<sub>2</sub> crystals. It indicates that the BCs appeared with the disappearance of aggregates.

In fact, our previous studies showed that for small nanocrystals the growth of SnO<sub>2</sub> via the classical dissolution–precipitation process was very slow.<sup>10</sup> In addition, throughout the process from 180 h (abundant with ~350 nm aggregates) to 280 h (abundant with ~350 nm BCs), we could seldom see SnO<sub>2</sub> crystals of intermediate size between ~10 and ~350 nm, when ignoring the small part of SnO<sub>2</sub> much smaller than 350 nm. On the basis of the above evidence, we conclude that BCs suddenly formed on the basis of aggregates as the precursor. Hence, an attempt was made to compare the size distribution and shape between the aggregates and BCs. As for the size, statistics (histogram of Figure 2f) reflect that the newly formed BCs are of an average size of ~350 nm, close to the original aggregates as previously shown at 180 h. Enlarged SEM images in Figure S3 (SI) also demonstrate that the shapes of BCs are similar to those of the original aggregates. This supports the standpoint that the aggregates are the precursor of the BCs.

**Model of Fast Growth Kinetics.** On the basis of the growth characteristics of SnO<sub>2</sub> stated above, the route of BC formation is proposed as shown in Figure 3. In the first stage of slow NP growth ( $\leq 180$  h in 250 °C series), a large number of NPs aggregate with each other to form an aggregate. In the second stage ( $>180$  h in 250 °C series), a fast crystal occurs by the fusion of the aggregates to form SnO<sub>2</sub> BC of similar size

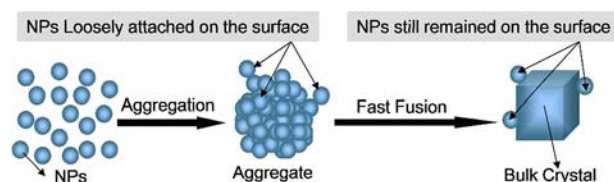


**Figure 3.** Aggregation-induced fast crystal growth model. First, hundreds of thousands of NPs attached to form a submicrometer aggregate. Second, fast crystal growth occurs by the fusion of aggregates to form a BC of similar size and shape. A layer of small NPs can be found attached on the surface of the BC.

and shape. When taking the aggregate and SnO<sub>2</sub> bulk crystal as  $\alpha$  and  $\beta$ , respectively, the fast growth process can be represented by the following equation



where  $k$  is the reaction rate constant.

The reaction order (more general, the rate law) is closely related to the intrinsic mechanism. The fast growth from  $\alpha$  to  $\beta$  within a short period of time resembles the well-characterized reaction of radioactive decay of atomic nucleus such as uranium, which is typically a first-order reaction. On the basis of this, we assume reaction 1 to be first-order. Accordingly, the decrease in the content of  $\alpha$  over time can be written as

$$v = -\frac{d[\alpha]}{dt} = \frac{d[\beta]}{dt} = k[\alpha]$$

Thus,

$$k = \frac{1}{t} \ln \frac{[\alpha]_0}{[\alpha]}$$

and

$$t_{1/2} = \frac{\ln 2}{k}$$

where  $t_{1/2}$ , half-life, is the time it takes for the content to fall from  $[\alpha]_0$  to  $[\alpha]_0/2$ . In a first-order reaction, plotting  $\ln[\alpha]_0/[\alpha]$  against time  $t$  should give a straight line with a slope of  $k$ . In this work

$$\frac{[\alpha]_0}{[\alpha]} = \frac{[\alpha]_0}{[\alpha]_0 - [\beta]} = \frac{1}{1 - \frac{[\beta]}{[\alpha]_0}}$$

Thus, it can be written as

$$k = \frac{1}{t} \ln \frac{1}{1 - \frac{[\beta]}{[\alpha]_0}}$$

where  $[\beta]/[\alpha]_0$  represents the relative amount of BCs with respect to the original SnO<sub>2</sub> aggregates that can convert to BCs completely. As shown in Table S1 in the SI,  $[\beta]$  is the relative amount of BCs with respect to the SnO<sub>2</sub> nanoparticles, as plotted in Figure 1d. These nanoparticles consist of aggregates and dispersed nanoparticles as well. As seen from Figure 1d, the relative amount of dispersed nanoparticles was ~25%. On the basis of this, the initial amount of aggregates relative to that of all the SnO<sub>2</sub> nanoparticles,  $[\alpha]_0$ , is ~75%. Hence, as shown in Table S1 (SI), the value of  $[\beta]/[\alpha]_0$  can be figured out, and  $k$  can be calculated.

By substituting  $[\beta]/[\alpha]_0$  into the above equation, a plot of  $\ln[\alpha]_0/[\alpha]$  against time  $t$  gives a straight line, as shown in

Figure 4. The graph is also linear when the coarsening temperature was set at 263 °C, while the onset of the fast

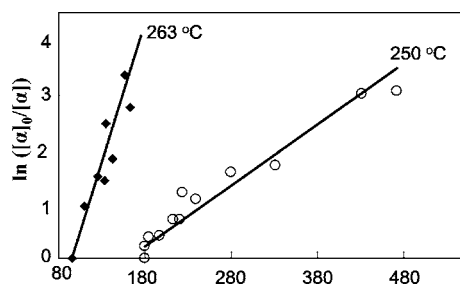


Figure 4. Plots and fitting results of  $\ln([\alpha]_0/[\alpha])$  against the coarsening time at 250 and 263 °C, respectively.

growth starts about 100 h earlier as compared to that of 250 °C. This demonstrates that the reaction 1 is first-order. Table 1

Table 1. Estimated Values by Fitting the Experimental Data at Each Temperature

temperature (°C)	$K$ ( $\text{h}^{-1}$ )	$t_{1/2}$ (h)
250	0.011	63
263	0.056	12

shows the fitted data involving the reaction rate constant and half-life  $t_{1/2}$  at each temperature. A decrease in  $t_{1/2}$  demonstrates that the higher the temperature, the faster the transformation rate from  $\alpha$  to  $\beta$ .

Although only two sets of kinetic constant vs temperature data are available (Table 1), it is possible to estimate the activation energy ( $E_a$ ) and the pre-exponent factor ( $A_0$ ) based on the Arrhenius equation

$$\ln K = -\frac{E_a}{RT} + \ln A_0$$

Or

$$E_a = \frac{T_1 T_2}{T_2 - T_1} R \ln \frac{K_2}{K_1}$$

where  $R$  is the universal gas constant (8.314 J/mol K), and  $T$  is the absolute temperature. In the narrow temperature range ( $T_2 - T_1 = 13$  K), we assume that both the  $E_a$  and  $A_0$  are independent of the temperature. The estimated  $E_a$  and  $A_0$  were determined to be 291.8 kJ/mol and  $1.53 \times 10^{27} \text{ h}^{-1}$ , respectively. Although the activation energy is higher than that required for simple OA growth of nano-SnO<sub>2</sub> ( $E_{a(\text{OA})} = 49.7$  kJ/mol),<sup>10</sup> the pre-exponent factor is much higher than that in the latter. This means that once the aggregation-induced growth is initiated by enough thermal fluctuation it proceeds drastically and is much faster than a simple OA.

## DISCUSSION

Apparently, the formation of aggregates is the prior and crucial step for the steep crystal growth of SnO<sub>2</sub>. As shown in Figure S7 (SI), SEM investigation of time series samples before and after the fast growth in our work indicates that numerous aggregates of small SnO<sub>2</sub> NPs already formed in the system from the beginning of the coarsening process. Nevertheless, temperature series experiments suggest that the fast growth of aggregates only happened after a threshold time of 180 and 100 h for 250 and 263 °C, respectively. It indicates that changes in

the state of aggregates should take place in the initial stage (first hundred hours). Normally, a hydrothermal environment can result in both the growth of nanoparticles and the evolution of aggregates. Interestingly, the kinetic data shown in Figure S1 (SI) and Figure 2a clearly demonstrate that in the initial stage little change can be found in either the morphology or particle size of SnO<sub>2</sub> NPs, the building blocks of the aggregates. In this case, it is probably the change in the aggregation state of aggregates that finally gives rise to the fast growth. To verify this, time series SAXS data of SnO<sub>2</sub> treated hydrothermally were collected and analyzed (refer to Figure S8 (SI)). The fractal dimensions of SnO<sub>2</sub> aggregates were derived from the SAXS data, which can be used to infer how dense the aggregates are (i.e., the aggregation degree). Figure 5 shows

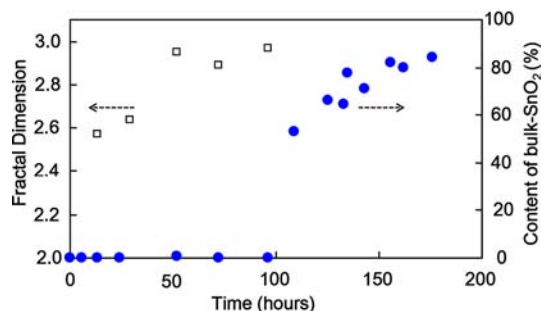
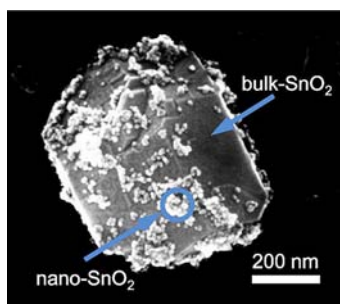


Figure 5. Relative content of bulk-SnO<sub>2</sub> in the sample versus time during the hydrothermal treatment in water at 263 °C, as well as the change in fractal dimension of aggregates versus time.

both the fractal dimension of the aggregates and the content of BCs in samples versus time after the hydrothermal treatment at 263 °C. An increasing fractal dimension of the aggregates from 2.5 to 3 can be seen. In principle, a low fractal dimension  $\sim 2.5$  at 13 h indicates loose aggregates in primary particles. A higher fractal dimension at longer time indicates that the aggregates are denser. When the fractal dimension approaches 3 at 96 h, the aggregates are rather dense. It should be noted that the fast growth occurred around 100 h right after the formation of the densest aggregates. This implies that the onset of the fast growth is closely related to an increasing aggregation degree of the aggregates. Therefore, we define the fast growth observed in SnO<sub>2</sub> as an aggregation-induced fast crystal growth. The decrease of surface energy is conventionally assumed as the driving force for the growth of small nanocrystals via OR or OA.<sup>6,8,15</sup> In spite of the challenge in directly probing the process of how the fast growth proceeds from the aggregates to the BCs, it is reasonable to assume the driving force for this process to be a reduction in surface free energy accomplished by complete removal of pairs of surfaces among nanoparticles.

Considering the degree of aggregation to be a key factor, those NPs in relatively disperse state should not grow fast via such a route. Experimental details confirm this assumption. As shown in Figure 1d, about a quarter of SnO<sub>2</sub> NPs in the sample hardly transformed into BCs (i.e., they just remained at several nanometers), even when the coarsening process proceeded for a long time. As shown in Figure 2c, these SnO<sub>2</sub> NPs were in a relatively disperse state compared to the aggregates shown in Figure 2d. This is further confirmed by the fact that most newly formed BCs are covered by a layer of residual NPs at 280 h (Figure S3b (SI)). The explanation of this phenomenon is illustrated in Figure 3. For a big aggregate, NPs on the surface layer of the aggregate could be relatively looser than the inner

ones. Once fast crystal growth occurs in the core of the aggregates, the NPs on the surface layer cannot grow and transform into BCs. When the coarsening time was prolonged long enough to 472 h, as shown in Figure 6, small SnO<sub>2</sub> NPs



**Figure 6.** SEM image showing a bulk-SnO<sub>2</sub> crystal in the sample after coarsening in water at 250 °C for 470 h. A few small nano-SnO<sub>2</sub> can still be found attached on its surface.

can still be found scattered on the surface of adjacent BCs. Furthermore, TEM analysis demonstrates that there is little change in the particle size in this time period (Figure S9 (SI)). Therefore, the scattered SnO<sub>2</sub> NPs could not grow big, supporting our proposed aggregation-induced fast crystal growth mechanism.

In principle, an aggregation-induced fast crystal growth mechanism could probably be inhibited by the breakup of the dense aggregates. To verify this, Al<sub>2</sub>O<sub>3</sub> of an initial size ~55.6 nm was introduced as a disperser to break the high aggregation state of SnO<sub>2</sub>, and the growth behavior of SnO<sub>2</sub> in this situation was investigated. Figure 7a and c shows the XRD pattern and TEM image, respectively, of SnO<sub>2</sub> treated by Al<sub>2</sub>O<sub>3</sub> and coarsened at 250 °C for 670 h. SnO<sub>2</sub> was scattered on the surface of Al<sub>2</sub>O<sub>3</sub>, as shown in Figure 7c. Both XRD and TEM confirm that all SnO<sub>2</sub> nanoparticles are only ~8 nm with

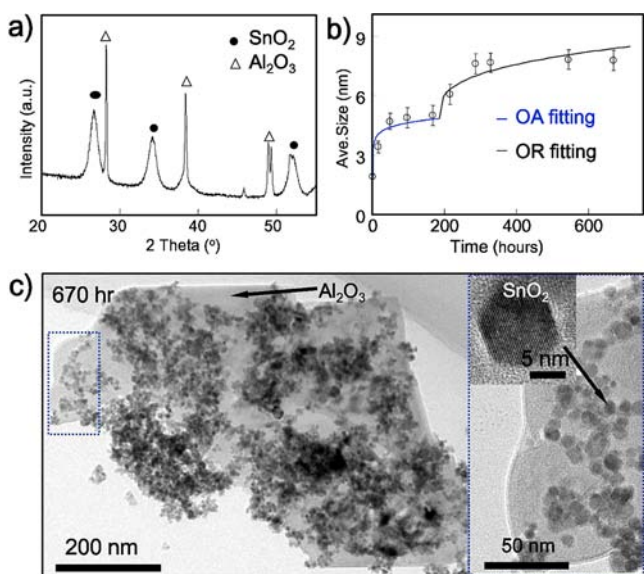


**Figure 7.** (a) XRD pattern of nano-SnO<sub>2</sub> dispersed and coarsened in the environment of Al<sub>2</sub>O<sub>3</sub> and water at 250 °C for 670 h and (b) the corresponding stepwise increase of particle size of nano-SnO<sub>2</sub> versus time. (c) A typical TEM image of the sample at 670 h clearly demonstrates that numerous nano-SnO<sub>2</sub> scattered on the surface of bulk Al<sub>2</sub>O<sub>3</sub> crystals. No SnO<sub>2</sub> BCs can be found.

neither large aggregates nor BCs. Figure 7b shows the particle sizes of SnO<sub>2</sub> nanoparticles versus coarsening time. In this case, SnO<sub>2</sub> started to grow via OR at ~180 h following the growth via OA before ~180 h. There was no big jump (from nanometers to hundreds of nanometers) in the particle size, though the particle size increased in two steps (Figure 7b). The particle size can still be considered as continuous throughout the coarsening process.

## CONCLUSIONS

A steep growth of nanocrystals from ~4 to ~350 nm was observed in hydrothermal growth of SnO<sub>2</sub> nanoparticles, which presented growth characteristics of “either small or large” in the particle size. An aggregation-induced fast crystal growth mechanism was proposed to explain this novel growth mode. Kinetic analysis, for the first time, indicates that the steep growth from aggregates to BCs is a first-order reaction with respect to the content of the aggregated nanoparticles. SAXS data support that the onset of the fast growth is related to an increase in the aggregation degree of the aggregates, driven by the reduction in the surface free energy. Breaking the aggregate can inhibit the steep growth, leading to a stepwise increase of particle size usually found in traditionally OA + OR crystal growth. This new aggregation-induced crystal growth mechanism may be employed to synthesize novel crystals of other materials.

## ASSOCIATED CONTENT

### Supporting Information

Growth kinetics of SnO<sub>2</sub> at 250 °C within 0–180 h; XRD data processing by Rietveld Refining method; detailed TEM and SEM information of samples; SAXS analysis of nano-SnO<sub>2</sub> aggregates; data for first-order kinetic fitting. This material is available free of charge via the Internet at <http://pubs.acs.org>.

## AUTHOR INFORMATION

### Corresponding Author

[zlin@fjirsm.ac.cn](mailto:zlin@fjirsm.ac.cn); [heng@eps.berkeley.edu](mailto:heng@eps.berkeley.edu)

### Notes

The authors declare no competing financial interest.

## ACKNOWLEDGMENTS

Financial support was provided by the National Basic Research Program of China (2010CB933501, 2013CB934302), the Outstanding Youth Fund (21125730, 50625205), the National Science Foundation Grant (20971123, 21273237, 21007070, 21103191, 51102232), the Knowledge Innovation Program of the Chinese Academy of Sciences (KJXC2-YW-N50, KJXC2-EW-J02), and the Fujian Science Foundation Grant (2010J06006, 2012J05035). H.Z. acknowledges financial support provided by the U.S. National Science Foundation (EAR-0920921) and U.S. Department of Energy (DE-AC02-05CH11231).

## REFERENCES

- (1) Hyeon, T.; Lee, S. S.; Park, J.; Chung, Y.; Bin Na, H. *J. Am. Chem. Soc.* **2001**, *123*, 12798.
- (2) Puentes, V. F.; Krishnan, K. M.; Alivisatos, A. P. *Science* **2001**, *291*, 2115.
- (3) Peng, X. G.; Wickham, J.; Alivisatos, A. P. *J. Am. Chem. Soc.* **1998**, *120*, 5343.
- (4) Lin, Z.; Gilbert, B.; Liu, Q. L.; Ren, G. Q.; Huang, F. *J. Am. Chem. Soc.* **2006**, *128*, 6126.

- (5) Huo, J.; Wang, L.; Irran, E.; Yu, H. J.; Gao, J. M.; Fan, D. S.; Li, B.; Wang, J. J.; Ding, W. B.; Amin, A. M.; Li, C.; Ma, L. A. *Angew. Chem., Int. Edit.* **2010**, *49*, 9237.
- (6) Wagner, C. Z. *Elektrochem.* **1961**, *65*, 581.
- (7) Zhang, J.; Huang, F.; Lin, Z. *Nanoscale* **2010**, *2*, 18.
- (8) Penn, R. L.; Banfield, J. F. *Science* **1998**, *281*, 969.
- (9) Zhang, J.; Lin, Z.; Lan, Y. Z.; Ren, G. Q.; Chen, D. G.; Huang, F.; Hong, M. C. *J. Am. Chem. Soc.* **2006**, *128*, 12981.
- (10) Zhuang, Z. Y.; Zhang, J.; Huang, F.; Wang, Y. H.; Lin, Z. *Phys. Chem. Chem. Phys.* **2009**, *11*, 8516.
- (11) Huang, F.; Zhang, H. Z.; Banfield, J. F. *Nano Lett.* **2003**, *3*, 373.
- (12) Zhan, J. H.; Lin, H. P.; Mou, C. Y. *Adv. Mater.* **2003**, *15*, 621.
- (13) Yu, D. B.; Sun, X. Q.; Zou, J. W.; Wang, Z. R.; Wang, F.; Tang, K. *J. Phys. Chem. B* **2006**, *110*, 21667.
- (14) Liu, W. Z.; Huang, F.; Liao, Y. Q.; Zhang, J.; Ren, G. Q.; Zhuang, Z. Y.; Zhen, J. S.; Lin, Z.; Wang, C. *Angew. Chem., Int. Ed.* **2008**, *47*, 5619.
- (15) Zheng, X. J.; Kuang, Q.; Xu, T.; Jiang, Z. Y.; Zhang, S. H.; Xie, Z. X.; Huang, R. B.; Zheng, L. S. *J. Phys. Chem. C* **2007**, *111*, 4499.
- (16) Banfield, J. F.; Welch, S. A.; Zhang, H. Z.; Ebert, T. T.; Penn, R. L. *Science* **2000**, *289*, 751.
- (17) Yuwono, V. M.; Burrows, N. D.; Soltis, J. A.; Penn, R. L. *J. Am. Chem. Soc.* **2010**, *132*, 2163.
- (18) Colfen, H.; Mann, S. *Angew. Chem., Int. Ed.* **2003**, *42*, 2350.
- (19) Kim, C.; Noh, M.; Choi, M.; Cho, J.; Park, B. *Chem. Mater.* **2005**, *17*, 3297.
- (20) Ristic, M.; Ivanda, M.; Popovic, S.; Music, S. *J. Non-Cryst. Solids* **2002**, *303*, 270.
- (21) Lee, E. J. H.; Ribeiro, C.; Longo, E.; Leite, E. R. *Chem. Phys.* **2006**, *328*, 229.
- (22) Ribeiro, C.; Lee, E. J. H.; Longo, E.; Leite, E. R. *ChemPhysChem* **2005**, *6*, 690.